Journal of Materials Research and Technology 37 (2025) 4382–4395

Contents lists available at ScienceDirect

Journal of Materials Research and Technology

journal homepage: www.elsevier.com/locate/jmrt

Effect of preparation conditions on the properties of ZIF-8@ZnO PEO coating

Valeryia Kasneryk [a,b,*], Hauke Rohr [c], Qianqian Chen [a,d], D.C.Florian Wieland [e], Anton Davydok [f], Eugen Gazenbiller [a], Maria Serdechnova [a], Carsten Blawert [a], Norbert Stock [c,g], Mikhail L. Zheludkevich [a,g,h]

[a] Institute of Surface Science, Helmholtz-Zentrum Hereon, Max-Planck-Straße 1, 21502, Geesthacht, Germany
[b] Erlangen Center for Interface Research and Catalysis, Friedrich-Alexander-Universität Erlangen-Nürnberg, Egerlandstraße 3, 91058, Erlangen, Germany
[c] Institute of Inorganic Chemistry, CAU Kiel University, Max-Eyth-Straße 2, D-24118, Kiel, Germany
[d] Corrosion and Protection Center, Northeastern University, 3-11 Wenhua Road, Shenyang, 110819, China
[e] Institute of Metallic Biomaterials, Helmholtz-Zentrum Hereon, Max-Planck-Straße 1, 21502, Geesthacht, Germany
[f] Institute of Materials Physics, Helmholtz-Zentrum Hereon, Notkestraße 8, 22607, Hamburg, Germany
[g] Kiel Nano, Surface and Interface Science (KiNSIS), Kiel University, Christian-Albrechts-Platz 4, D-24118, Kiel, Germany
[h] Faculty of Engineering, CAU Kiel University, Kaiserstraße 2, 24143, Kiel, Germany

ARTICLE INFO

Handling editor: P Rios

Keywords:
Plasma electrolytic oxidation
Metal organic framework
ZIF-8
Multifunctional coating
Corrosion protection

ABSTRACT

Recently, metal organic frameworks (MOFs), crystalline porous materials, demonstrated their effectiveness for the post-modification of coatings obtained by plasma electrolytic oxidation (PEO) treatment. The post-modification leads to the sealing of PEO porosity as well as endowing the coating with active corrosion protection ability. In the current work, ZnO-based PEO coatings on the surface of Z1 Zn alloy was partially converted into ZIF-8 by treatment with vapours of 2-methylimidazole (2-HmIm). It was found that the degree of PEO-to-ZIF-8 conversion and the size of the ZIF-8 particles increased with an increase in temperature from 120 to 150 °C, and with an extension of the treatment with 2-HmIm from 5 h to 60 h. Furthermore, the sealing of the PEO pores can be controlled by applying different treatment conditions. It was also found that such treatments resulted in the enhancement of the corrosion resistance of the materials. However, the key factor determining the performance of the final ZIF-8@PEO hybrid coatings was a balance between the level of ZnO-based PEO dissolution and crystallisation of ZIF-8 phase.

1. Introduction

Nowadays, multifunctional coatings possessing several functions at the same time are being actively developed due to their beneficial properties [1–5]. In this context, coatings obtained by plasma electrolytic oxidation (PEO) are of interest to numerous researches [6,7]. These coatings are formed on the surfaces by applying short living micro-discharges generated at high voltages, that leads to local heating, melting and oxidation of the metals [8–11]. Applying the PEO technique to Al- [12–15], Mg- [16–22], Ti- [8,23–25] and Zn-based [26–28] materials enables the formation of highly adhesive, mechanically strong ceramic-like oxide layers on their surfaces. PEO coatings have already demonstrated their potential for use in wear and corrosion protection. Furthermore, the potential applications of PEO coatings have been also expanded to include photocatalytic and biomedical areas, where they demonstrate high levels of biocompatibility and antibacterial activity [29–34]. However, the main feature of the PEO coatings is their highly porous structure. Numerous pores can spread throughout the coatings [35] and, as a result, impair their protective ability. In the context of corrosion protection, this is disadvantageous and consequently, hinders the further industrial integration of the PEO coatings. Conversely, this highly developed pore system represents an outstanding macro-container, i.e., the system that can be used for further post-synthesis loading with functional species, enabling the tuning of PEO coating properties or even the implementation of new functionalities.

In this regard, the development of post-modification with corrosion inhibitors, such as decylphosphonate [36], 3-methylsalicylate [37],

* Corresponding author. Institute of Surface Science, Helmholtz-Zentrum Hereon, Max-Planck-Straße 1, 21502, Geesthacht, Germany.
E-mail address: valeryia.kasneryk@hereon.de (V. Kasneryk).

https://doi.org/10.1016/j.jmrt.2025.07.038
Received 5 June 2025; Received in revised form 4 July 2025; Accepted 6 July 2025
Available online 7 July 2025

8-hydroxyquinoline [20,38], 1,2,4-triazole and benzotriazole [39] is underway. It enables the introduction of active corrosion protection into the PEO coatings. Even more, Gnedenkov et al. demonstrated that post-sealing PEO layers with 8-hydroxyquinoline can significantly increase the antibacterial activity of the MA8 magnesium alloy [20]. Another example is the design of a biodegradable surface with a drug delivery function, as reported by Bordbar-Khiabani et al., who post-modified a PEO coating on the AZ91 Mg alloy with betamethasone sodium phosphate [40]. However, it should also be mentioned, that the biggest disadvantage of these systems is the uncontrolled release of functional species during application.

A more advanced approach, which is currently the focus of numerous research groups working in the field of post-modification for PEO coatings, is the "container-in-container" method. This method involves the sealing the PEO pores with nanocontainers, i.e. nanomaterials that can intercalate, store and release different functional species in a controlled manner [41,42]. In this context, the use of layered double hydroxides (LDHs) nanocontainers has been widely studied [43–51]. This strategy involves growing LDH flakes on the upper surface and inside the PEO pores followed by the intercalating corrosion inhibitors into the LDH structure. This approach has been successfully applied to PEO coatings formed on the surface of AA2024 Al [52,53], AZ31 [54–56], MA8 [57], and ZK60 [58] Mg alloys. As a result, self-healing coatings that can inhibit corrosion processes on demand were obtained.

As an alternative to LDH for the sealing of PEO pores, metal organic frameworks (MOFs), materials belonging to the class of coordination polymers with highly regular porous networks, are attracting increasing attention [59–63]. The increased interest is due to their range of features, including variable pore size, large porosity, multiple functionalities and compatibility with a wide range of different materials. To date, the post-modification of PEO layers on the surface of Z1 Zn [64] and AZ31 [65] or AZ91D [66] Mg alloys with ZIF-8 has been the main focus of interest. ZIF-8 is a zeolitic imidazolate framework structure composed of Zn^{2+} ions interconnected by 2-methylimidazolate ions (2-mIm^-) [67–72]. Following the decoration of the PEO layers, the ZIF-8 crystals can effectively seal the PEO pores, thereby improving the barrier properties of the coatings. They can also act as a source of inhibitors (2-methylimidazolate) endowing the coating with the ability of active corrosion protection properties [73]. Moreover, it has been demonstrated that ZIF-8 can also adjust the photocatalytic and photoluminescence properties of $ZnO/ZnAl_2O_4$-based PEO coatings on Z1 Zn alloy [64].

In our previous investigation, the development of a novel technique for the formation of ZIF-8@PEO hybrid coatings on Z1 Zn alloy, known as vapour-solid transformation (VST), was reported [74]. The Z1 Zn alloy is widely used in the construction industry for producing roofing materials, gutters, downpipes etc. Furthermore, Z1 Zn alloy found application for the production of non-structural components for various industries, including automotive, hardware, electronics etc [75]. In turn, the formation of multifunctional coatings on its surface can facilitate and/or develop new areas of industrial application. The VST is a technique based on the controllable partial transformation of PEO layers into ZIF-8 in the presence of 2-HmIm under solvent-free conditions. This transformation was found to run through a multistage mechanism involving the partial dissolution of the PEO layers, accompanied by the formation of new defects on the surface. The released zinc ions then reacted with the organic ligands to form ZIF-8, whose crystallisation began on the PEO surface and gradually spread into the internal PEO pores. This seals the PEO pores and defects with ZIF-8 and, resulting in the formation of a compact protective coating. The current investigation aims to understand how the VST conditions affect the ZIF-8 phase distribution throughout the PEO coating, and how this influences the coating's corrosion resistance and photocatalytic properties.

2. Experimental part

2.1. Materials

30 x 20 x 1 mm^3 zinc alloy sheets (Z1, according to EN988, VMZinc) were used as the substrate. The alloy had the following composition [wt. %]: 0.08–1 % Cu, 0.06–0.20 % Ti, 0.02 % Pb, 0.002 % Cd, 0.001 % Sn, ≤0.015 % Al, and Zn balance.

2.2. Preparation of the parental PEO coatings

The parental PEO coatings were formed on the surface of Z1 Zn alloy (sheets with a size of 30 x 20 x 1 mm^3, surface area of 22 cm^2), similar to the procedure reported in Ref. [74]. For this, a pulsed DC power supply under a voltage of 300 V and current limits of 2 A (current density of 92 mA/cm^2) with a pulse ratio of t_{on}:t_{off} = 1 ms:9 ms was used. The experiment was conducted by connecting Z1 Zn alloy specimens to function as the anode, with a stainless steel tube from the cooling system serving as the cathode. The PEO coatings were prepared for 5 min under continuous stirring at a temperature of 20 ± 2 °C, which was maintained by a circulating external water-cooling system. The applied electrolyte contained 2 g/l potassium hydroxide (KOH, >99 %, Sigma-Aldrich Chemie GmbH), and 10 g/l trisodium phosphate (Na_3PO_4, techn., Alfa Aesar). The obtained specimens were rinsed with distilled water and dried in air.

2.3. Preparation of ZIF-8@PEO coatings

ZIF-8@PEO coatings were synthesised via vapour-solid transformation (VST). Details of the treatment are presented in Refs. [74,76]. In short, PEO coated specimens placed vertically were treated with 50 mg of 2-methylimidazole (2-HmIm, TCI, >97 %) organic linkers at temperatures of 120 °C, 140 °C or 150 °C for 5 h, 20 h 40 h or 60 h in a 30 ml autoclave. The specimens were labelled as T-t, where T refers to the treatment temperature and t to the treatment time. A table of the prepared specimens is provided in the SI (Table SI–1).

2.4. Characterisation

The phase composition of the parental PEO and ZIF-8@PEO coatings was evaluated by X-ray diffraction (XRD, Ni filtered Cu Kα radiation source, Bruker D8 Advance, Germany). Analysis was performed at a glancing angle of 3°, within a scan range from 5 to 50° and at a step size of 0.02° and a scan speed of 1 s per step.

The surface morphology and cross-sections of the initial PEO and obtained T-t coatings were analysed using a scanning electron microscope (SEM, Tescan Vega3 SB, Czech Republic) equipped with an energy dispersive X-ray spectrometer (EDX, Ultim Max 40, Oxford, UK). Surface morphology was examined in secondary electron (SE) mode. Cross-sections of the coatings were studied in back scattered electron (BSE) mode. Data acquisition was performed at high voltages of 11.0 kV–15.0 kV and a beam intensity of 10.0–14.0. Prior to the cross-section analysis, the Z1 Zn plates coated with PEO or ZIF-8@PEO were embedded in resin, ground with silicon carbide paper (#1200, #2500 and #4000), washed with distilled water, and dried in air. Before the measurement, the materials were sputtered with carbon. The size of the ZIF-8 particles, the thickness of the coatings and the surface porosity were estimated from the SEM micrographs (magnifications: 200x, 500x and 2000x, respectively) using ImageJ software [77].

The distribution of crystal phase across the PEO and ZIF-8@PEO coatings was evaluated at the nano-focus end station at the P03 beamline of the PETRA III storage ring at the Deutsches Elektronen-Synchrotron (DESY, Germany) [78]. The experimental set-up is presented in detail in the reference [79]. Data were acquired using an Eiger 9 M detector with a pixel size of 75 μm by 75 μm. The X-ray beam had an energy of 19.7 keV and was focused to a beam size of 1.5 μm by 1.5 μm

by means of KB mirrors. A mesh scan was performed across the interface of the coatings on an 80 × 80 μm area: 40 steps perpendicular to the interface with a 2 μm step size, and 20 steps parallel to the interface with a step size of 4 μm. The acquisition time was 1 s for each step. Azimuthal integration was done using PyFai [80] and two-dimensional analysis of the diffraction profiles was done using an in-house developed Matlab routine.

The corrosion protective ability of PEO and ZIF-8@PEO coatings was evaluated by electrochemical impedance spectroscopy (EIS) with a Gamry Interface 1000 potentiostat (Gamry, Warminster, USA). Testing was carried out using a conventional three electrode cell, which included PEO- and ZIF-8@PEO-coated specimens with an exposed surface area of 0.5 cm^2 as working electrodes, a Pt wire as the counter electrode, and a saturated Ag/AgCl reference electrode. Experiments were conducted in a 0.5 wt% NaCl solution at 22 °C, within a frequency range from 100 kHz to 0.1 Hz at open circuit potential (OCP) with 10 mV RMS sinusoidal potential perturbations. The EIS measurements were performed after the following immersion times: 1, 3, 6, 12, 24, 72, and 168 h. To demonstrate the reproducibility of the data, each type of specimen was evaluated for three times.

The photocatalytic activity of the initial PEO and ZIF-8@PEO coatings was evaluated using photodegradation of methyl orange (MO, ACS reagent) dye as a model reaction. Prior to the photocatalytic tests, the samples were cut into 1 x 1 cm^2 size pieces and activated at 100 °C for 3 h under reduced pressure. The photocatalytic tests were performed in a photocatalytic reactor (Photocube ThalesNano, Hungary) in UV mode (365 nm, 100 %). The specimens were placed into 5 ml of 8.8 mg/l MO solution in water and treated at 22 °C for 6 h. In parallel with the photocatalytic tests, the adsorption properties of the coatings were evaluated by stirring under dark conditions. MO concentrations were determined by UV–Vis spectroscopy (Shimadzu UV-2600i, Japan) based on an MO calibration curve (0.96–9 mg/L).

3. Results and discussions

3.1. Optimisation of the VST conditions for preparation of ZIF-8@PEO coatings: XRD study

Our previous study showed that the VST technique was effective in forming ZIF-8@ZnO PEO coatings on the surface of Z1 Zn alloy [74]. ZIF-8 crystallisation occurred not only on the upper surface of the coatings, but also inside the PEO pores, effective sealing them. In the current study, the VST conditions were systematically varied to understand their effect on the properties of the final ZIF-8@PEO coatings. Prior to the VST treatment, PEO coatings were produced on the Z1 Zn alloy surface using the conditions reported in Refs. [74,81]. The resulting coatings were mainly composed of ZnO (*PDF: 00-001-1136)* as the main phase, with $Zn_2P_2O_7$ (PDF: PDF 00-001-0841) detected by XRD as the secondary phase (Fig. 1).

At the next stage, the as-prepared ZnO-based PEO coatings were treated with 50 mg of 2-HmIm in an autoclave, with the temperature and treatment time systematically varied. Fig. 1 shows the XRD patterns for the three batches of specimens obtained at 120, 140 and 150 °C. As it can be seen, ZIF-8 was the main phase formed during transformation at all three temperatures. Reflections corresponding to ZnO were also present in the patterns, indicating that the treatment conditions did not allow for a complete transformation of the PEO layers. Alongside the ZIF-8 reflections, a signal appeared at 10.9° 2θ in the XRD patterns of all T-t coatings, demonstrating the formation of an unknown admixture phase. Even more, the reflection at 8.7° 2θ was also detected in the XRD pattern of 120-60, which can correspond to the $C_{32}H_{40}N_{16}Zn_4$ phase (PDF: 00-060-1335) (Fig. 1, a). It should also be emphasised that this admixture formed even after numerous repetitions of the process at 120 °C for 60 h.

The ZnO PEO-to-ZIF-8 recrystallisation process was affected by both temperature and VST time. Firstly, regardless of the applied temperature, the ZIF-8 formation was observed after 5 h of VST. The intensity of the ZIF-8 reflections increased with treatment time from 5 h to 40 h, while the intensity of the ZnO reflections decreased for all three batches. A similar effect was observed when the VST temperature increased from 120 to 150 °C; this can be seen by comparing the diffraction patterns of the T-20 or T-40 coatings. Among the three batches, reflections of the ZIF-8 phase in the XRD patterns of 150-20 or 150-40 were significantly higher than those obtained at 120 and 140 °C for 20 and 40 h, respectively. This indicates that increasing the VST temperature accelerates the ZnO-to-ZIF-8 transformation. However, whereas the intensities of the ZIF-8 reflections further increased for 120-60 and 140-60 compared to 120-40 and 140-40, respectively, for the 150-60 specimens (Fig. 1, c), they slightly dropped. This observation could indicate the termination of the transformation process due to a deficiency of the 2-HmIm linker, either because it has been consumed or because it can not diffuse to the surface of the PEO coating due to ZIF-8 particles, as discussed previously in Ref. [74]. Moreover, it could be associated with partial flaking off of the ZIF-8 layer from the surface, as observed in Ref. [64].

3.2. SEM study of ZIF-8@PEO surface morphology

The surface morphology of the initial PEO and the obtained T-t coatings is presented in Fig. 2. The initial PEO coating formed on the Z1 Zn alloy has a porous structure, which is typical of the PEO coatings (Fig. 2, a)). The size of the pores on the PEO surface varied from 1 to 60

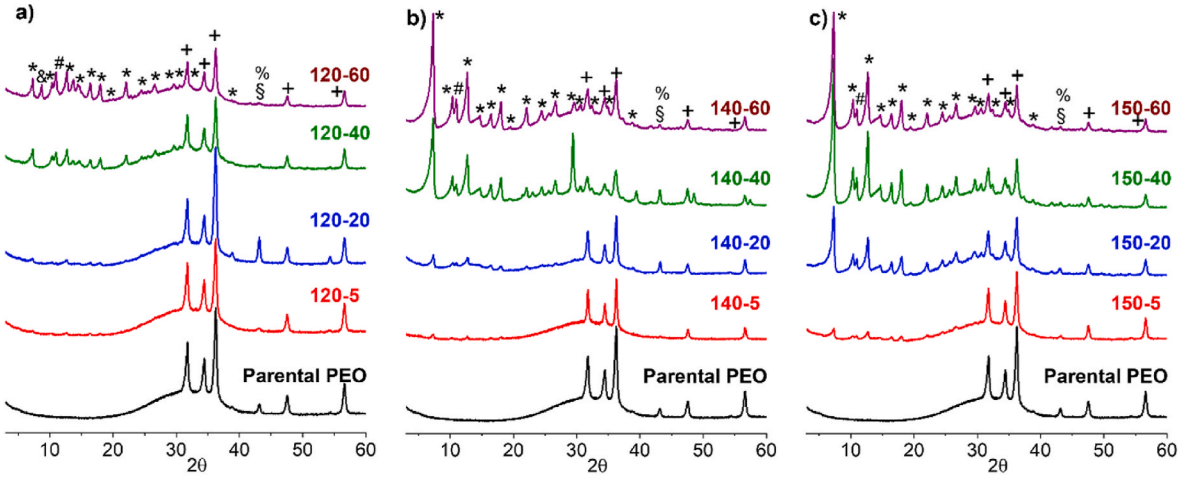

Fig. 1. XRD patterns of ZIF-8@PEO coatings prepared by the VST approach at a) 120 °C, b) 140 °C and c) 150 °C for 5, 20, 40 and 60 h + - ZnO, * - ZIF-8, + % - $Zn_2P_2O_7$, § - Zn, & - $C_{32}H_{40}N_{16}Zn_4$ and # - unknown admixture phase.

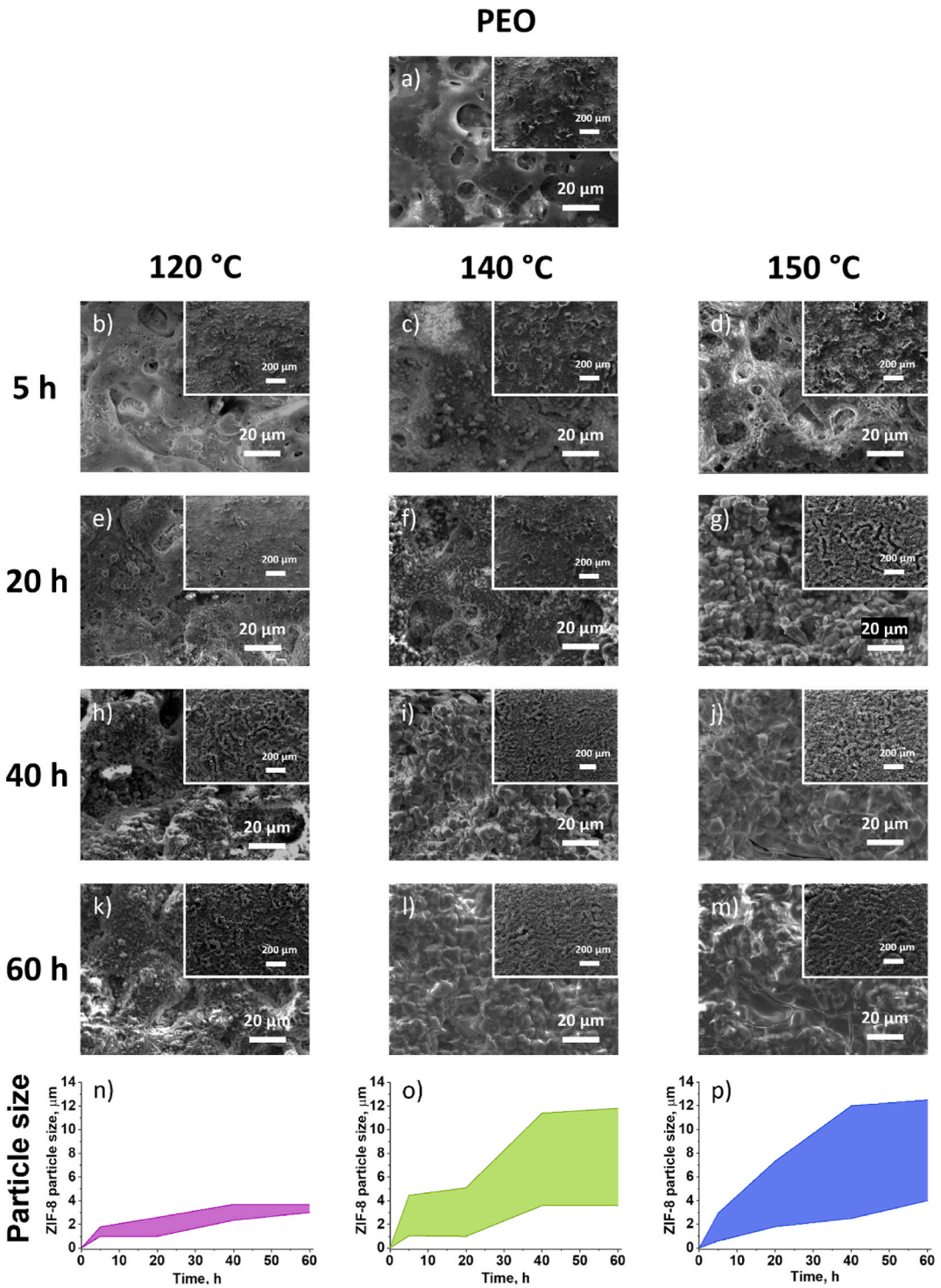

Fig. 2. a)-m) SEM micrographs of the obtained T-t specimens. The inserts show the high-magnification images of the surface. n)-p) Distribution of ZIF-8 particle size (from minimum to maximum values estimated from SEM images using ImageJ software) showing the samples prepared at 120–150 °C over time.

μm. Following the transformation treatment, the surface porosity changed, and these modifications depended strongly on the applied VST conditions. Firstly, the SEM image of the 120-5 specimen (Fig. 2, b)) shows that the surface porosity of the PEO coating increased compared to the initial coating, with values of 21.3 ± 2.1 vs. 18.3 ± 1.3 %, respectively (Table 1). At the same time, the presence of ZIF-8 particles can already be detected on the surface of the PEO coatings. SEM images of the specimens prepared at 5 h, but at elevated temperatures, (i.e., 140-5 and 150-5; Fig. 2, c), d)), already revealed a high level of sealing

Table 1
Surface porosity for the initial PEO coating and T-t specimens (%) estimated from SEM micrographs.

	120, °C	140, °C	150, °C
5 h	21.3 ± 2.1	11.0 ± 0.5	9.9 ± 0.5
20 h	13.7 ± 1.8	9.6 ± 0.5	9.6 ± 0.7
40 h	12.7 ± 0.8	8.0 ± 1.4	7.2 ± 0.2
60 h	11.7 ± 0.7	7.1 ± 0.6	8.3 ± 1.7
PEO	18.3 ± 1.3		

of the surface pores. Thus, the surface porosity decreased to the values of 11.0 ± 0.5 % and 9.9 ± 0.5 % for the 140-5 and 150-5 specimens, respectively. Furthermore, increasing both the temperature and the time of the VST process resulted in decreased surface porosity, which was associated with the sealing of the pores by active formation and growth of ZIF-8 particles. However, the highest level of the PEO pores' sealing was observed for the 140-40, 140-60 and 150-40 samples, which is indicated by the surface porosity of 8.0 ± 0.6 %, 7.1 ± 0.6 % and 7.2 ± 0.2 %, respectively (Table 1). It should be noted that, despite the 150-60 coatings demonstrated comparable pore sealing values (i.e., 8.3 ± 1.7 %), high-magnification SEM micrographs show that treatment at these conditions (i.e. 150 °C for 60 h) caused new cracks and surface defects to form. This was most likely due to the stresses created in the layer by ZIF-8 particles growing in all directions on the PEO coating surface.

Variation in VST parameters also impacted the shape and the size of the ZIF-8 particles. Only a few poorly shaped ZIF-8 particles with a size of 1.0–1.8 μm, and distributed inhomogenously across the surface can be seen in the SEM image of 120-5 (Fig. 2, b). The number of particles increased when the treatment was prolonged to 20 h (Fig. 2, e). They are mainly similar in size, with some measuring up to 2.6 μm. In the case of 120-40, most of the ZIF-8 particles were still poorly shaped, and only a few had recognisable shapes. These particles reached a size of 3.7 μm (Fig. 2, h). However, in contrast to 120-5 and 120-20, the coating surface was homogeneously covered by ZIF-8. Further prolongation of the VST treatment up to 60 h mainly affected the size and the shape of the ZIF-8 particles. In that case, they were well-formed and grew to a size of up to 3.0 μm (Fig. 2, k).

Increasing the VST temperature to 140 °C resulted in the ZIF-8 particles enlarging further and increasing in their number. Thus, all specimens showed a homogeneous covering of the surface with ZIF-8, with size ranging from 1.0-4.4 μm to 3.0–11.8 μm for 140-5 and 140-60, respectively (Fig. 2c–f, i, l). However, while the shape of the particles can be easily followed for 140-5, 140-20 and 140-40 (i.e. rhombic dodecahedron morphology typical of ZIF-8), the surface of 140-60 appeared to be covered with sintered particles. A similar tendency was observed for the batch of the coatings, which were prepared at 150 °C. Thus, the SEM images of these specimens show, that the PEO surface was fully covered by the particles with a size of 0.6–2.9 μm, 1.8–7.2 μm, 2.5–12.0 μm and 4–12.5 μm for 150-5, 150-20, 150-40 and 150-60 coatings (Fig. 2d–g, j, m), respectively. Similarly to the 140-60 coatings, the ZIF-8 particles looked intergrown on the surfaces of the 150-40 and 150-60 coatings (Fig. 2j–m).

3.3. Surface elemental composition of the coatings by EDX

EDX analysis was performed to evaluate the elemental composition of the ZIF-8@PEO coatings. Figs. 3–5 represent the EDX elemental mappings for the 120-t, 140-t and 150-t systems, respectively. Zn, O and P are relatively homogenously distributed across the surface of the parental PEO coating formed on the Z1 Zn alloy (Fig. 3). Following the treatment with 2-HmIm, areas with a higher Zn concentration were observed, indicating the location of the ZIF-8 particles. Treatment time had a strong effect on the distribution of N, O and P on the top surface of the coatings. N was unevenly located on the surfaces of specimens treated for short periods (5 and 20 h) with small areas of high concentration being particularly evident in the 150-5 material (Fig. 5).

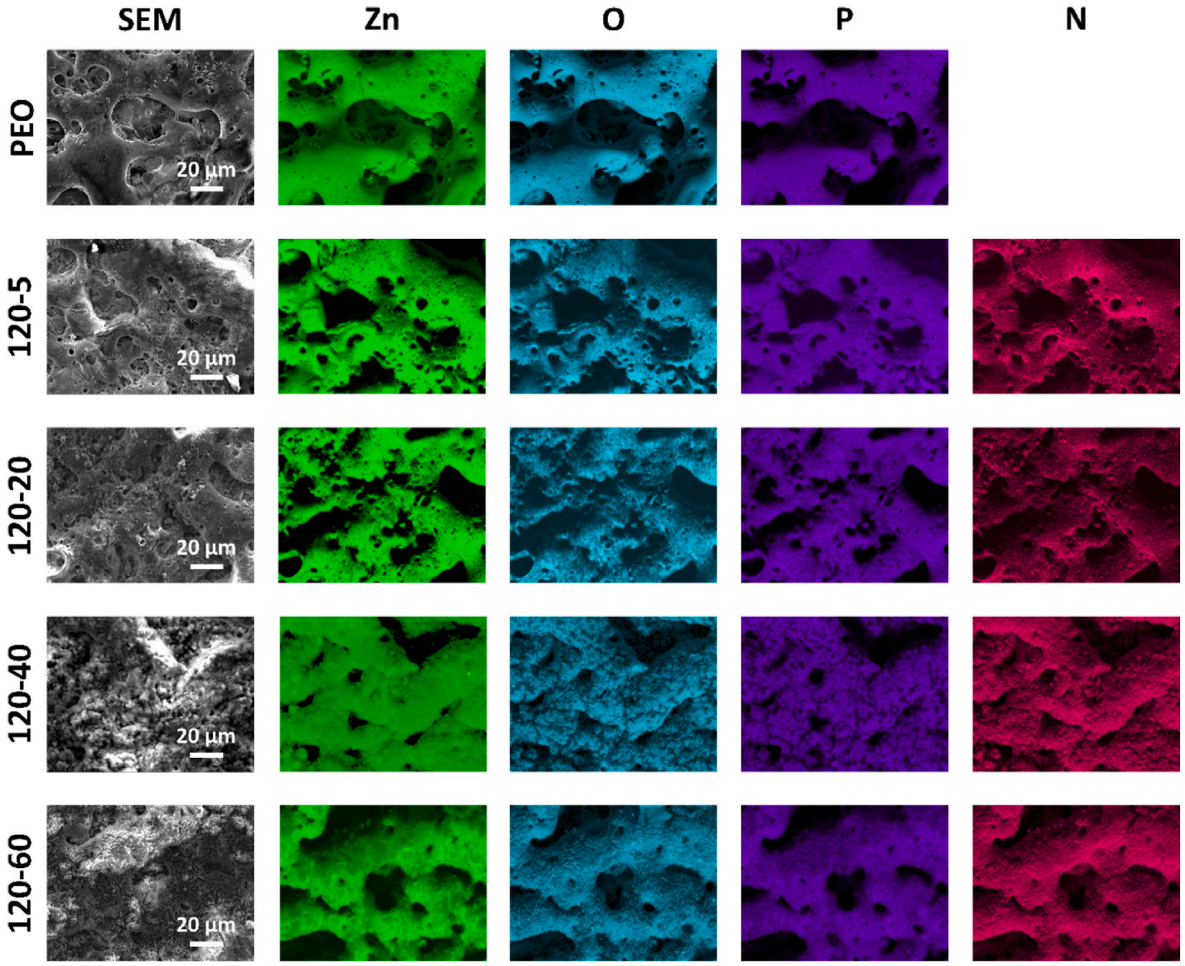

Fig. 3. Results of EDX elemental mappings for the parental PEO coating and the specimens from the 120-t batch.

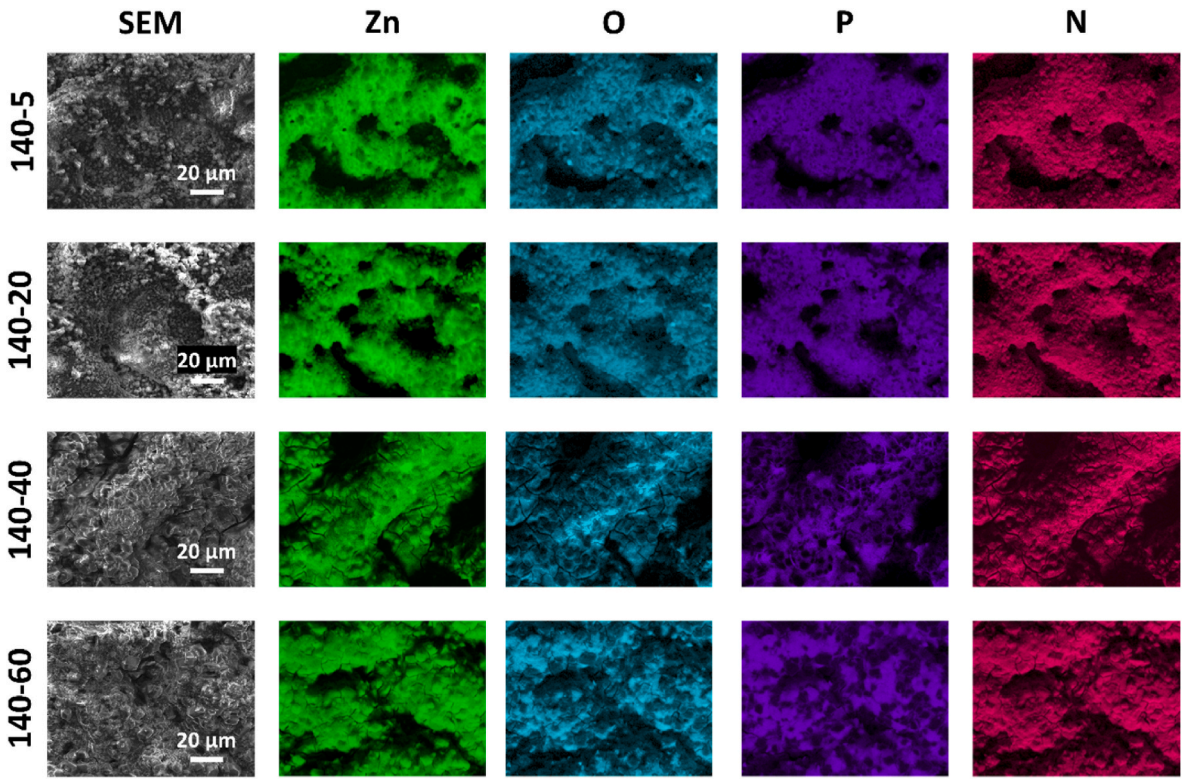

Fig. 4. Results of EDX elemental mappings for the specimens from the 140-t batch.

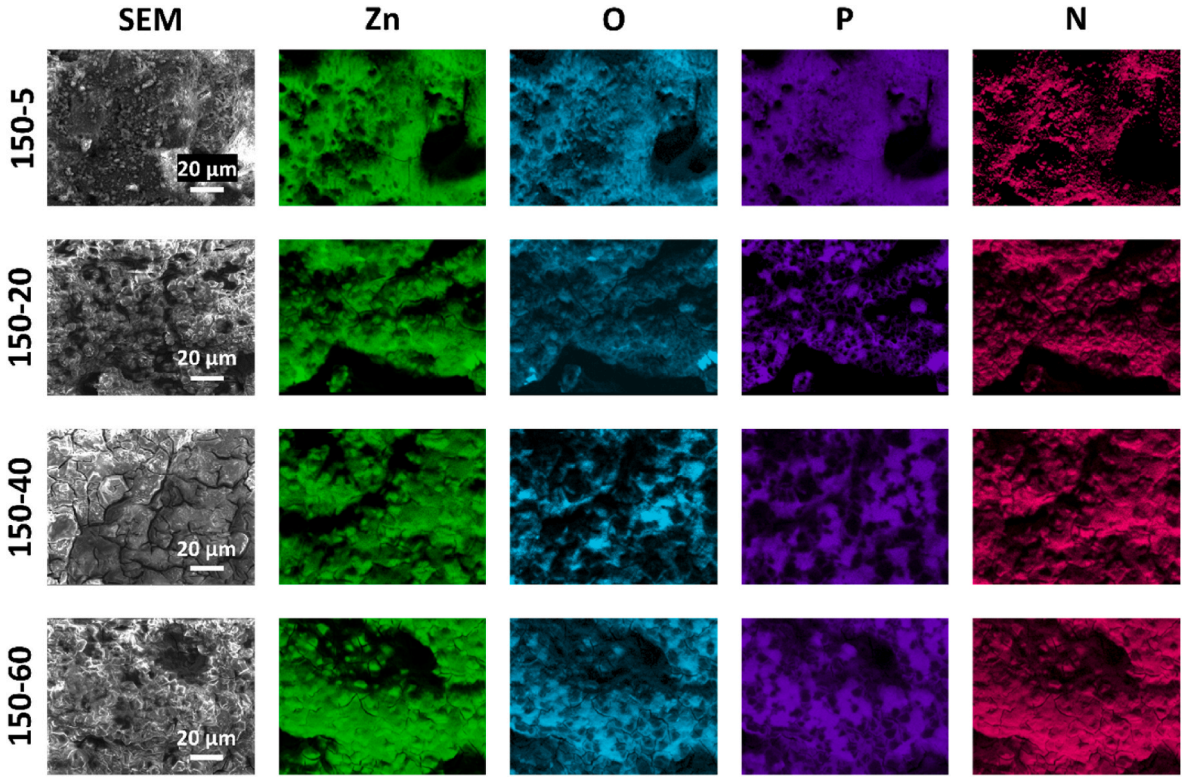

Fig. 5. Results of EDX elemental mappings for the specimens from the 150-t batch.

Specimens obtained after 40 h and 60 h showed a more uniform distribution of N on the surface. In the case of allocation of O and P, the longer the PEO coatings were treated with 2-HmIm, the more irregular the distribution of these elements on the surfaces became. This is particularly evident in the EDX mapping of the T-40 and T-60 materials. Based on the SEM images, the surfaces of these coatings' surfaces exhibit a high level of pore sealing. The O and P mappings appeared „meshy", as can be seen in the EDX images of the 150-40 and 150-60 plates (Fig. 5).

This is associated with a high level of ZIF-8 crystallisation on the PEO surface in coatings that have undergone longer treatment. The exception was the 120-60 coating. However, this sample showed the presence of admixtures, as proven by XRD analysis.

Table 2 lists the chemical composition of the initial PEO coatings and ZIF-8@PEO specimens. The concentrations of Zn, P and O decreased mainly with the prolongation of the VST transformation, while the amount of N increased on the surface. A similar trend is evident when comparing the samples obtained at the same treatment times, but at different temperatures. Thus, the N content (wt. %) increased from 9.60 ± 0.02 to 16.58 ± 0.03 with an increase in VST time from 5 h to 60 h at 120 °C, from 14.91 ± 0.03 to 22.06 ± 0.03 at 140 °C and from 11.29 ± 0.02 to 22.55 ± 0.03 at 150 °C. These observations correlate with the results of the XRD results, which demonstrate that the ZIF-8 phase crystallises more readily with an increase in both VST time and temperature. It should also be mentioned, that clear trend emerges from the carbon concentration data. The variation in C concentration in the specimens might be due to the way the samples were prepared and their subsequent exposure to air.

3.4. Elemental and phase distribution through the coatings

To understand how the VST conditions affect the distribution of elements and main phases within the coatings perpendicular to the surface, elemental mapping of the cross-sections was carried out using SEM/EDX and nano-focused synchrotron X-ray diffraction analyses. Based on the SEM cross-section analysis, the thickness of the initial ZnO-based PEO coating ranged from 5 μm to 45 μm (Fig. 6, Fig. SI–1). This significant variation in PEO thickness is most likely related to variations in the distribution of current density during the process, leading to different growth rates in different areas. The PEO layer structure was relatively dense, containing pores of various sizes located on the external part of the coating and in the inner layer close to the metallic substrate. Similarly to the EDX mapping of the top view (Fig. 3), the cross-sectional mappings also confirmed the homogeneous distribution of Zn, O and P elements throughout the initial PEO layer.

Treatment with 2-HmIm linkers had little effect on the thickness of most final T-t coatings, which ranged from 4 μm to 50 μm. This slight variation from the initial PEO coating value can be associated with consecutive transformation of the PEO layer and deposition of ZIF-8 particles on the surface, as previously discussed in Ref. [74]. Local dissolution of the PEO layer can be observed in certain areas of the coatings. For the coatings obtained at elevated temperatures and longer reaction times, the thickness values increased up to 16–78 μm, as can be seen in the cross-section images of the 140-60, 150-40 and 150-60 samples (Figs. 7 and 8). This thickening was primary due the deposition of a large quantity of the ZIF-8 phase on the upper surface, as well as the enlargement of particles, as demonstrated by the SEM analysis of the upper surface of the coatings (Figs. 4 and 5). Furthermore, it is evident that these coatings consist of two layers: the residual PEO layer and the deposited ZIF-8 layer.

Table 2
Chemical compositions of the specimens by EDX, wt. %.

Sample	Zn, %	O, %	P, %	C, %	N, %
PEO	60.12 ± 0.02	27.12 ± 0.01	11.96 ± 0.01		
120-5	38.69 ± 0.02	19.06 ± 0.01	6.99 ± 0.00	28.51 ± 0.02	6.76 ± 0.02
120-20	35.06 ± 0.01	16.07 ± 0.01	6.20 ± 0.00	32.98 ± 0.02	9.60 ± 0.02
120-40	22.72 ± 0.02	12.32 ± 0.01	5.10 ± 0.01	40.27 ± 0.03	19.59 ± 0.03
120-60	26.32 ± 0.01	12.64 ± 0.01	5.07 ± 0.00	39.93 ± 0.02	16.58 ± 0.03
140-5	28.51 ± 0.02	10.93 ± 0.01	5.10 ± 0.01	40.55 ± 0.01	14.91 ± 0.03
140-20	28.10 ± 0.01	11.50 ± 0.01	5.10 ± 0.01	39.60 ± 0.02	15.50 ± 0.02
140-40	23.00 ± 0.02	10.00 ± 0.01	3.60 ± 0.00	43.10 ± 0.03	20.40 ± 0.04
140-60	22.43 ± 0.01	9.30 ± 0.01	3.85 ± 0.00	42.35 ± 0.02	22.06 ± 0.03
150-5	31.98 ± 0.02	14.03 ± 0.01	6.02 ± 0.00	36.67 ± 0.02	11.29 ± 0.03
150-20	24.32 ± 0.02	9.14 ± 0.01	3.64 ± 0.00	43.57 ± 0.03	19.32 ± 0.03
150-40	21.90 ± 0.01	9.80 ± 0.01	3.40 ± 0.00	44.20 ± 0.02	20.70 ± 0.03
150-60	21.02 ± 0.01	10.65 ± 0.01	3.35 ± 0.00	42.43 ± 0.02	22.55 ± 0.03

When discussing the impact of the VST conditions on the elemental distribution throughout the coatings, no significant changes were observed in the mappings of O and P. The Zn maps remained mainly unchanged for most of the coatings. Only in the case of the T-40 and T-60 samples, two Zn layers can be clearly distinguished: a denser one with a higher concentration Zn corresponding to the ceramic PEO layer, and a less dense one, where the Zn signal was less intense and associated with the presence of ZIF-8 particles. However, the distribution of ZIF-8 within the ZIF-8@PEO coatings can mainly be followed from the nitrogen maps. Therefore, comparing the N mappings from the 120-t batches shows that no ZIF-8 was detected in the 120-5 samples, and only a few dots of this phase were found in the 120-20 and 120-40 samples. It can be mainly associated with the inhomogeneous coverage of the PEO layers with the ZIF-8 particles on the surface, as well as the small size of the particles, which was previously observed by SEM of the top view of the coatings (Fig. 3). Homogeneous coverage of the PEO layers with the ZIF-8 phase was only detected for the 120-60 coatings. Meanwhile, the ZIF-8 phase was mainly located on top of the PEO layers, rather than within them. Such observation indicates that a temperature of 120 °C was not sufficient to seal the inner pores of the PEO layers, and prolonging the treatment did not improve the process. In turn, increasing the temperature to 140 °C and 150 °C resulted in the sealing of both the external pores located on top of the PEO layers and the internal pores. This was particularly evident in the 140-40, 140-60, 150-40 and 150-60 coatings, the N elemental mappings of which showed the presence of N throughout the coatings' thickness (Figs. 7 and 8).

Further evaluation of the initial PEO coatings and ZIF-8@PEO specimens across the layers was performed by synchrotron X-ray diffraction. Mesh scan analysis was performed for this purpose, enabling the location of the different phases within the coating at particular points to be followed. Similarly to the results of the laboratory XRD study, ZnO was the main phase forming parental PEO coating, while ZIF-8@PEO coatings contained both ZIF-8 and ZnO. Fig. 9 shows 2D maps based on the analysis of ZnO (100), ZIF-8 (110) and Zn (100) reflection intensities, which were used to determine the location of the substrate and consequently the thickness of the coatings. In all cases, the thicknesses of the materials obtained varied within the range of 20–80 μm, which differed slightly from the thicknesses values obtained by the EDX cross-section analysis. This inconsistency could be mainly due to the different experimental settings applied in both analyses. Thus, synchrotron XRD mappings only covered a small part of the coatings (80 x 80 μm), while EDX cross-sectional analysis allowed following larger regions of the specimens to be examined. Moreover, such difference could be associated with different sample preparation methods for both analyses. In the case of EDX cross-sectional analysis, it includes cutting the samples followed up embedding them in resin and grinding them. Consequently, this multi-step procedure could slightly affect coating structure and thickness. In contrast, synchrotron measurements only require the samples to be mounted on holders, meaning they remain intact.

Firstly, Fig. 9 shows that a homogeneous distribution of either the ZnO or ZIF-8 phases was not achieved, regardless of the applied treatment conditions. Secondly, regardless of the treatment temperature, it was found that the intensity of ZnO decreased with an increase in

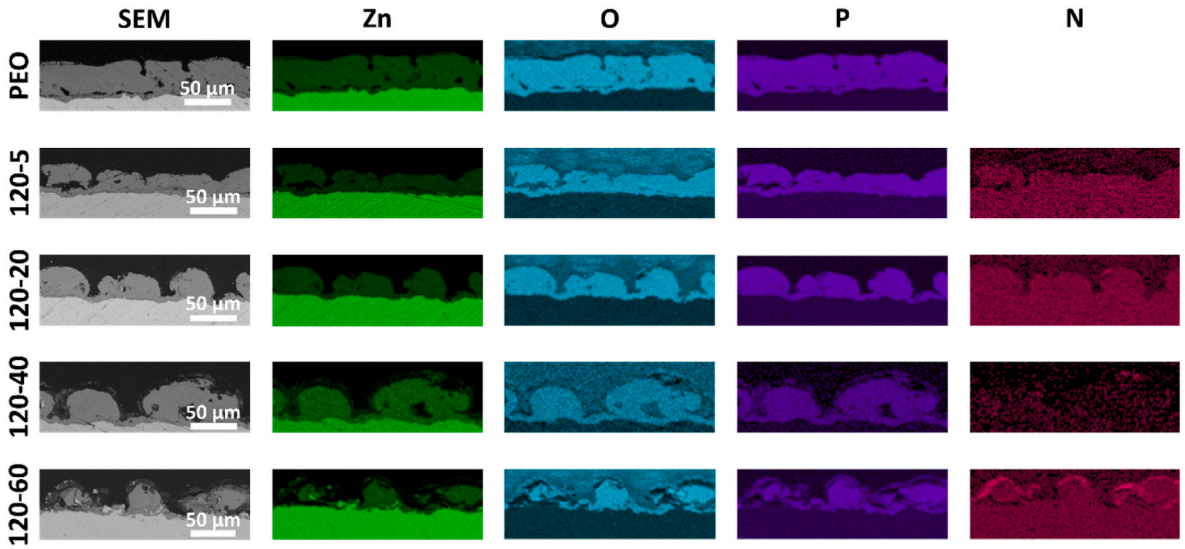

Fig. 6. SEM micrographs of the cross sections and elemental distribution for the parent ZnO based PEO coating and the 120-t coatings.

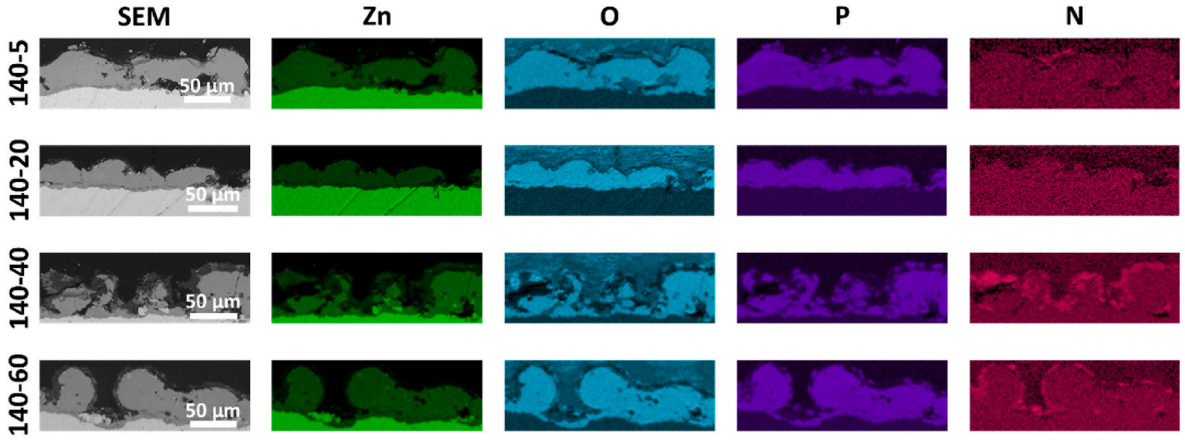

Fig. 7. SEM micrographs of the cross sections and elemental distribution for the 140-t coatings.

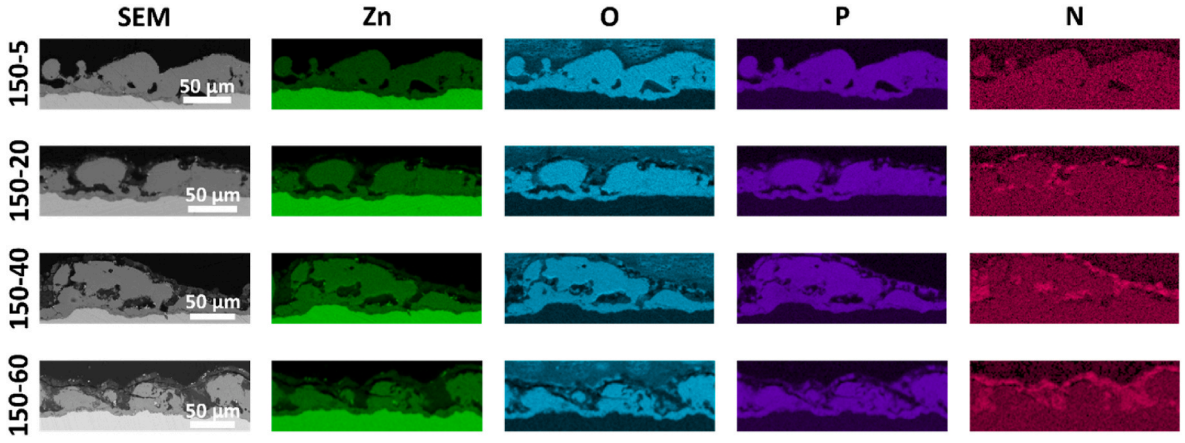

Fig. 8. SEM micrographs of the cross sections and elemental distribution for the 150-t coatings.

treatment time from 5 h to 60 h (for all three batches). This is consistent with the laboratory XRD results and can be associated with the ZnO-to-ZIF-8 transformation. In the case of the ZIF-8 phase, both treatment parameters, i.e. time and temperature, influenced its distribution. Thus, for the 120-t coatings, no strong signal indicating for the formation of ZIF-8 was detected for the specimen obtained for 5 h of treatment. This was most likely due to the inhomogeneous distribution and small size of the ZIF-8 particles (i.e., 1.0 μm–1.8 μm). Due to the use of a highly focused beam, the chance of hitting a particle is reduced, and, in addition, the scattering signal from a small particle is weak, which makes

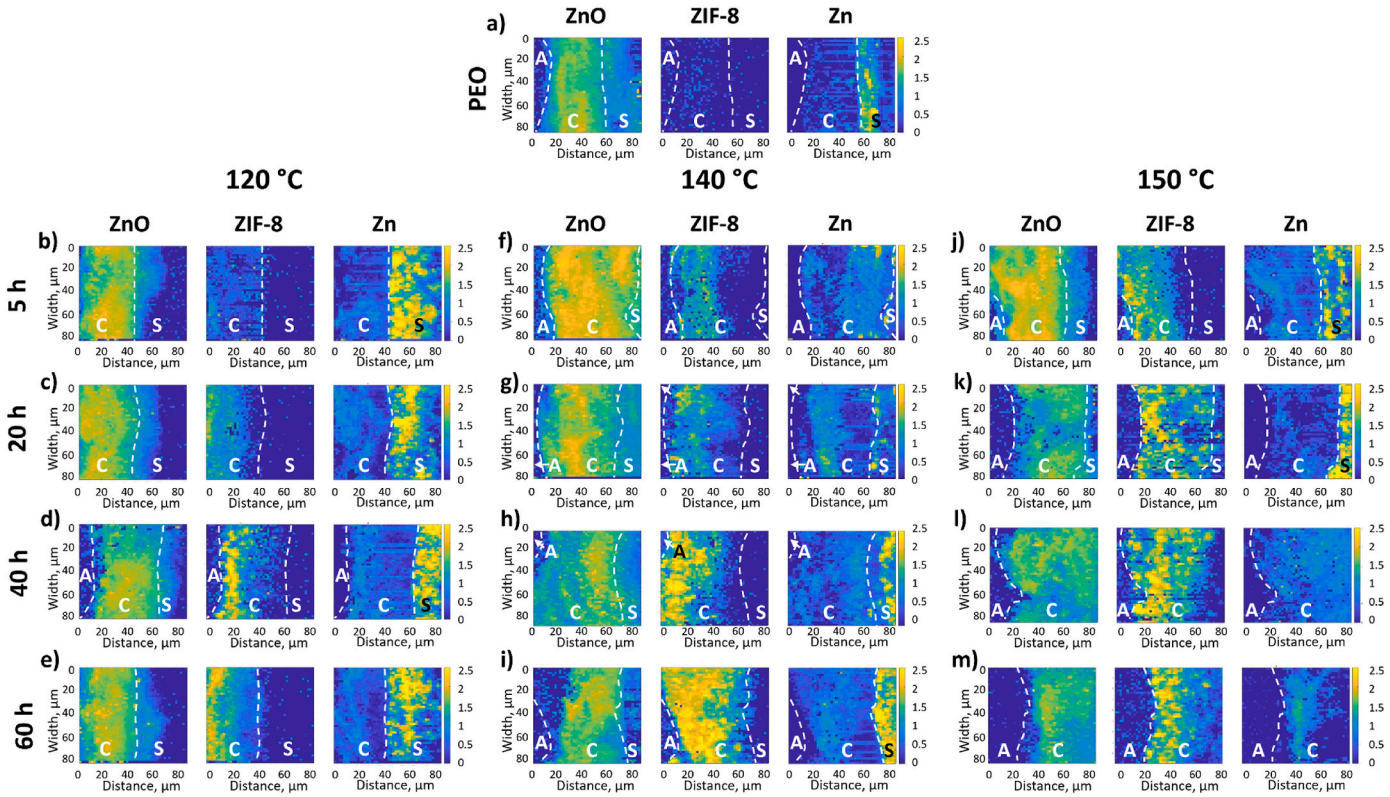

Fig. 9. 2D maps of ZnO, ZIF-8 and Zn phases distribution across a) PEO, b) 120-5, c) 120-20, d) 120-40, e) 120-60, f) 140-5, g) 140-20, h) 140-40, i) 140-60, j) 150-5, k) 150-20, l) 120-40, m) 120-60 coatings. **A, C** and **S** refer to the air, coating and substrate areas, respectively.

ZIF-8 detection challenging. A strong ZIF-8 signal was only detected for the 120-20 coating, and its intensity increased with the increase of treatment time up to 40 and 60 h. However, ZIF-8 was only present in the upper part of the coatings, was therefore not detected within the layers. This result is consistent with EDX cross-sectional analysis and confirms that a decreased temperature does not promote sealing of the PEO pores throughout the entire thickness of the coatings.

In the case of the coatings obtained at 140 and 150 °C, 2D mappings demonstrated the presence of the ZIF-8 phase in the coatings already after just 5 h of the treatment, which is consistent with the results of the XRD and SEM analyses (Figs. 1 and 2). Moreover, ZIF-8 concentration increases with increased VST time and temperature. The effect of temperature can be illustrated by comparing the 140-5 and 150-5 coatings. Thus, while the ZIF-8 phase was inhomogeneously distributed within both coatings, areas with a higher ZIF-8 concentration were clearly apparent in the 150-5 material. A similar effect was also observed with increased treatment time, as the amounts of ZIF-8 inside the coatings were higher for coating obtained through prolonged treatment, i.e., T-40 and T-60 (Fig. 9, h, i, l, m). Moreover, mapping of the 150-20, 150-40 and 140-60 coatings (Fig. 9i–k, l) revealed that the ZIF-8 phase was not only present on the surface of the coatings, but also in areas close to the substrate. Consequently, these observations confirm the positive effects of elevated temperatures and longer treatment times on sealing the PEO coating throughout its thickness.

3.5. *Evaluation of corrosion protection properties of the ZIF-8@PEO coatings*

The effect of the ZnO-to-ZIF-8 transformation on the protective ability of the Z1 Zn alloy was evaluated using electrochemical impedance spectroscopy (EIS) after the parental PEO plates and 140-t plates were immersed in a 0.5 wt % NaCl solution. The 140-t batch was selected for the evaluation based on the results discussed previously. Unlike the 120-t batch, homogeneous coverage of the PEO surface with ZIF-8 particles was achieved for all 140-t specimens. Conversely, no additional surface defects were formed compared to samples obtained at longer treatment at 150 °C (Fig. 2j–m). Fig. 10a–e) shows the Bode and phase angle plots after the immersion for 1–168 h, while corresponding Nyquist plots are presented in Fig. SI–2 (SI). The spectra demonstrate the presence of several relaxation processes in the parental PEO and ZIF-8@PEO coatings. However, not all the time constants can easily be distinguished due to overlap, particularly in the case of the ZIF-8@PEO spectra.

The EIS spectra of the initial ZnO-based PEO coatings grown on the surface of Z1 Zn substrate are characterised by the presence of four time constants. At the beginning of the immersion in corrosive media, the spectra contained a time constant of around 10^5 Hz. This high-frequency time constant is most likely due to the response of the porous part of the PEO coatings. The relaxation process observed at middle-frequencies (10^4 Hz) can be attributed to the response from the inner barrier layer of the PEO coating. At lower frequencies (about 10 Hz), another relaxation process is observed, which can be caused by the corrosion process. At very low frequencies (0.01 Hz), the relaxation, whose presence could be associated with electrochemical activities on the metallic surface, is visible. As the immersion time is prolonged from 12 h to 168 h, these time constants shift in terms of frequency and become even more depressed. The impedance modulus drops significantly in full frequency range, reaching the values below 10^3 Ω cm^2 at 0.01 Hz after just one day of exposure, suggesting low barrier properties and stability of the PEO layer as well as a high rate of corrosion processes. However, an increase in the impedance modulus was observed for the PEO sample when the immersion time was increased from 72 to 168 h, suggesting that pore sealing with corrosion products had taken place to some extent.

In contrast to the original PEO, the 140-5 specimen exhibits a significantly higher impedance level in the inner barrier layer. Although it drops very quickly over time, reaching levels similar to those of

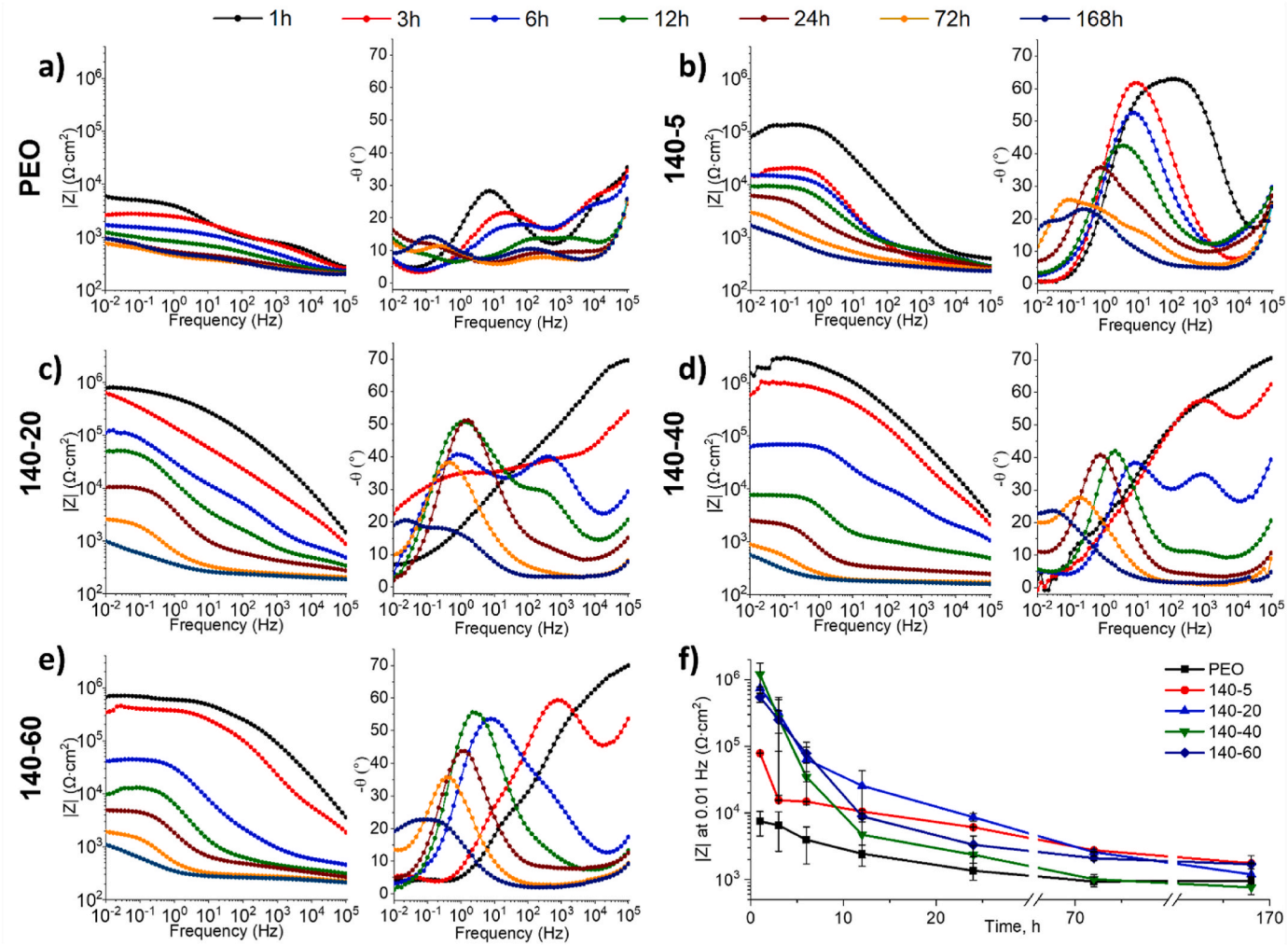

Fig. 10. Bode and phase angle plots for a) parental PEO, b) 140-5, c) 140-20, d) 140-40, e) 140-60 coatings grown on the surface of Z1 Zn alloy after the immersion in a 0.5 wt % NaCl solution for 1, 3, 6, 12, 24, 72 1nd 168 h. f) Evolution of |Z| at 0.01 Hz with an immersion time for PEO and ZIF-8@PEO coatings.

untreated PEO after comparable immersion periods. However, an important difference can be observed in the region related to corrosion processes, namely the significantly increased resistance associated to the charge transfer process.

In the case of samples prepared via the long post-treatment conversion process (20–60 h), changes in the spectra evolution are observed, which especially remarkable for the samples immersed for 1 h in 0.5 wt % NaCl. The identification of the processes in the spectra of 140-20, 140-40 and 140-60 coatings after 1 h of the immersion proved to be challenging. This observation could be associated with the limitation of the access of 0.5 wt % NaCl due to the high level of PEO pores sealing by ZIF-8 particles and consequently. In another words, it can thus be posited that the pores were only partially moistened. A similar effect was observed in the spectra of 140-20 after 3 h of immersion. Nonetheless, in all cases two time constants could be identified in the spectra: at approximately 10^5 Hz, this is most likely attributable to the response of the porous part of the PEO coatings in combination with ZIF-8; and at around 10^3–10^4 Hz, that is related to the response of the inner PEO layer. In turn, the presence of three time constants was followed in the 140-40 and 140-60 spectra after 3 h of the immersion in a 0.5 wt % NaCl. The nature of these relaxation processes is similar to those already described above for the original PEO and the one post-treated specimens for 5 h. Identifying all time constants in the spectra of the samples immersed for a long time, i.e., after 24–168 h, became again tricky, which is possibly associated with the dissolution of ZIF-8 from the upper surface and the pores and the PEO layer itself.

In order to compare the effect of the VST conditions on the protective ability of the ZIF-8 layer, |Z| at 0.01 Hz was plotted as a function of time (Fig. 10, f). $|Z|_{0.01}$ for the parental PEO was ~10^4 Ω cm^2 at the beginning of the immersion. It then decreased by one order of magnitude reaching a value around 10^3 Ω cm^2 (after 24 h of immersion), which demonstrated comparable values until the end of the immersion. Partial transformation of PEO-to-ZIF-8 even for 5 h of treatment time has a positive effect on the protective ability of the coatings. $|Z|_{0.01}$ was higher by around one order of magnitude throughout the whole period of the immersion in a 0.5 wt % NaCl solution. The corrosion resistance of the coatings was further improved with an increased VST reaction time of 20, 40 and 60 h. Thus, 140-20, 140-40 and 140-60 coatings resulted in the values of $|Z|_{0.01}$ around ~10^6 Ω cm^2. These values decrease with increased immersion time in corrosive media. However, while $|Z|_{0.01}$ has a value of ~10^5 Ω cm^2 after 12 h of EIS for 140-20, it was around ~10^4 Ω cm^2 for 140-40 and 140-60. In all three cases $|Z|_{0.01}$ continued to decrease with an increased exposure time to the corrosive solution. Finally, the values for all three coatings were comparable to those of the untreated PEO. However, while the $|Z|_{0.01}$ values for 140-20 and 140-60 coatings reached ~10^3 Ω cm^2 after 168 h, the $|Z|_{0.01}$ value for parental PEO sample had already dropped to the same value after 72 h and decreased slightly further (564 Ω cm^2 after 168 h).

3.6. Photocatalytic properties of ZIF-8@PEO coatings

Photocatalytically active surfaces are currently in the focus of numerous investigations as an alternative to traditional powder photocatalysts. The main area of interest relates to their potential application for wastewater treatment. In this context, the photoactivity of the obtained ZIF-8@PEO coatings was also evaluated. The photodegradation of MO under UV light was chosen as the model reaction. Alongside to the photocatalytic test, the obtained coatings were also treated with a MO solution in the dark to evaluate their adsorption abilities. Fig. 11 shows a comparison of the MO adsorption and photodegradation for the PEO and ZIF-8@PEO coatings after 6 h of exposure. Although the investigation focused on the 140-t batches, additional testing of 120-20 and 150-20 specimens was conducted to determine whether the temperature of the VST affected the MO adsorption and photoactivity properties.

The initial PEO coating exhibits relatively low photocatalytic activity for MO degradation. Only 28.6 % of MO was decomposed after 6 h of treatment, which is consistent with our previous investigation reported in Ref. [64]. However, it also exhibited a higher level of MO adsorption, namely 17.1 % of MO. Based on these results, it can be assumed that the real photocatalytic ability of untreated PEO coatings was even lower. It should also be mentioned, that such enhanced adsorption performance is generally considered to be rather negative, as adsorbed MO molecules can further block access of MO molecules to the active sites of photocatalysts.

Adsorption and photocatalytic activities decreased after partial transformation of PEO to ZIF-8. Comparing the adsorption properties among ZIF-8@PEO samples, the lowest value of MO adsorption, 4.9 %, was observed for the 140-20 material. A similar value of MO adsorption (5.9 %) was also found for the 140-60 coatings. For comparison, the percentages of the adsorbed MO were slightly higher for coatings prepared at shorter reaction times, i.e., 140-5, and other reaction temperatures, 120-20 and 150-20. 7.3, 9.3, 6.5 %, respectively. These results are strongly correlated with values of the surface porosity presented in Table 1 confirming that the decrease in the adsorption ability for ZIF-8@PEO materials was mainly associated with the sealing of the PEO porosity with ZIF-8 particles, and consequently blocking of MO adsorption in the inner part of the PEO coatings.

Comparing the effect of the condition of the PEO-to-ZIF-8 rearrangement on photocatalytic degradation of MO, 140-5, 140-20 and 120-20 samples exhibit similar results. Thus, the concentration of MO in the solutions decreased by only 9.2 % in the presence of these samples.

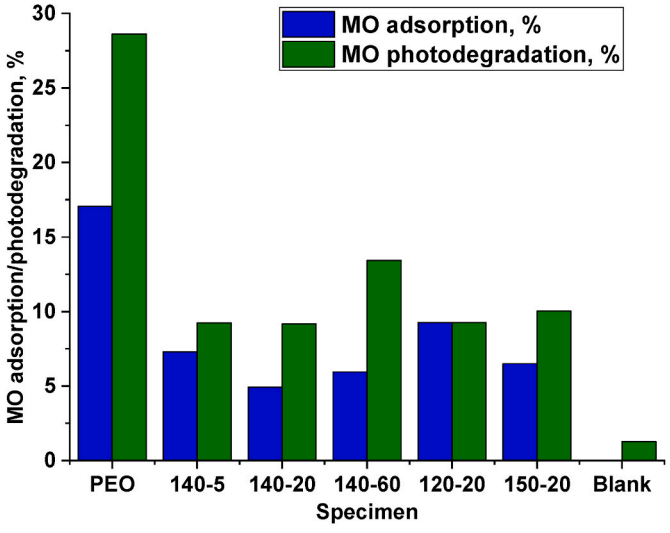

Fig. 11. MO adsorption and photocatalytic degradation of MO by the initial PEO and ZIF-8@PEO coatings from on Z1 Zn alloy after immersion in a 5 ml of 8.8 mg/l MO solution for 6 h.

The highest value in the decrease of MO concentration was observed for 140-60, reaching only 13.5 %. Such deteriorated behaviour of ZIF-8@PEO materials in MO photodegradation was generally unexpected and differed from our previous results on post-treatment of ZnO/$ZnAl_2O_4$ based PEO, where VST improved the performance of the parental coating by two times [81]. This decrease in MO photodegradation was also most likely due to the PEO coating being covered by ZIF-8 particles, which limits access of MO to ZnO, the compound mainly responsible for the photocatalytic activity of ZIF-8@PEO coatings (the ZnO bandgap is 3.2 eV vs. 4.9 eV for ZIF-8).

3.7. Discussion

Presently, post-modification of PEO with MOFs is regarded as a promising technology. This is due to the fact that it can provide effective sealing of PEO pores and enable the introduction of active corrosion protection in the coating. In our previous work, we reported on the possibility of post-modification of the PEO layer with ZIF-8 using the VST method. The VST as a technique has a range of advantages comparing to the solvothermal modifications. Firstly, the VST is a solvent-free approach. This prevents contamination of the PEO coatings and dissolution of the PEO layer by solvent, that is methanol or water in case of most ZIF-8 syntheses. Furthermore, the possible corrosion of the metallic surface by methanol similarly to reported in [82–84] is prevented. Moreover, the VST can be efficacious in sealing PEO pores of varying sizes. In contrast, the solvothermal growth of MOFs on the surface of PEO coatings grown on the surface of AZ31 Mg alloy [65,85] was reported to be insufficient for the effective sealing of the big size pores. And even more the formation of a highly porous upper layers is possible [66,85], whose barrier protection ability is limited.

The VST is a complex process involving several processes. It begins with the sublimation of the 2-HmIm linker present in the autoclave, which then reacts with ZnO, the main component of the PEO coating, to form crystalline ZIF-8 by the following reaction:

$$ZnO + 2HmIm \rightarrow Zn(mIm)_2 + H_2O$$

In order to understand how variations in VST conditions affect the characteristics and further performance of the final ZIF-8@PEO coatings, two main processes were followed: ZIF-8 crystallisation, and the effect of the transformation from PEO-to-ZIF-8 in and on the PEO layers.

Firstly, regardless of the applied treatment conditions, complete recrystallisation of the ZnO-based PEO layer into ZIF-8 did not occur. The present results are consistent with those obtained in our earlier study, which focused on the VST transformation of ZnO [74] and ZnO/$ZnAl_2O_4$-based PEO coatings [64]. Even more, as was reported in Refs. [76,86,87], the treatment of ZnO nanorods or films under conditions analogous to those reported in the current publication did not permit the complete transformation of the nanorods or films into ZIF-8. Such observation can be related to the fact that ZIF-8 particles, that grow on the top and inside the PEO pores, can obstruct diffusion of 2-HmIm linkers to ZnO and, consequently, terminate further recrystallisation. Conversely, this observation can be explained by the depletion of 2-HmIm in the reactor over time. However, as demonstrated in our previous investigation [74], increasing the amount of 2-HmIm in the VST (100 mg vs. 50 mg in the current work), did not result in complete PEO-to-ZIF-8 transformation.

Secondly, the VST conditions were critical for the sealing of the internal and external pores of the PEO coating. Based on the SEM top view and cross section analyses, as well as 2D synchrotron mappings, treatment at 120 °C was effective for sealing neither the surface nor the internal PEO pores and even the coatings obtained with long reaction times (i.e., 120-60) still contained a high number of original PEO pores. As presented in Table 1, the surface porosity was estimated to be 11.7 ± 0.7 % vs. 18.3 ± 1.3 % for the 120-60 and the initial PEO samples, respectively. This is related to the fact that at this reaction temperature,

ZIF-8 particles growth was limited. Despite numerous ZIF-8 particles being located on the upper surface of the coating, their size (with a maximum value of 3.7 μm) was insufficient for effectively sealing the large pores of the parental PEO layer with sizes up to 60 μm. In contrast to the results obtained at 120 °C, applying the VST to the PEO coatings at 150 °C resulted in the fast formation of ZIF-8 particles, further particle growth, and effective sealing of the PEO pores throughout the entire coating. However, this fast growth of ZIF-8 on the upper surface was also accompanied by cracks in the particles. It was most likely related to the space limitations for the ZIF-8 particles, i.e., mechanical stress in the layer caused by the growth of the ZIF-8 in all directions. Such cracks represent new surface defects that can provide fast access for the corrosive media to the metallic surface, and consequently provoke corrosion processes. In this context, 140 °C is the optimum reaction temperature for the formation of ZIF-8@PEO coatings. On the one hand, the nucleation and growth of ZIF-8 particles are relatively fast, providing effective PEO pore sealing. VST for 5 h–40 h allowed effective sealing of the surface pores, while long-term treatment (60 h) also led to the crystallisation of ZIF-8 inside the PEO layer (Fig. 9, i). On the other side, the surface remained dense even after long-term treatment with no cracking of the particles was detected in any of the materials in the batch.

Discussing the effect of the partial transformation of PEO layers into ZIF-8 on the coating performance, an improvement in corrosion resistance was observed. All coatings from the 140-t batches showed enhanced protection ability in a 0.5 wt % NaCl solution compared to the parental PEO samples. However, as shown in Fig. 10, f), the corrosion resistance of ZIF-8@PEO coatings decreased, becoming comparable to that of the PEO coating after 168 h of immersion was. Generally, the porous PEO layers provide a certain barrier protection for the metallic surface. ZIF-8, in turn, is an excellent nanocontainer of 2-HmIm corrosion inhibitors, that can be released into the medium upon the ZIF-8 decomposition, forming an adsorption layer on the metallic surface [64]. Application of VST results in the partial transformation of the PEO layer, and, therefore, decreases its barrier ability, while ZIF-8 formation can implement active corrosion protection for the coating, as previously mentioned, and consequently improve corrosion resistance. Moreover, ZIF-8 particles improve the barrier properties of PEO by sealing the pores. However, ZIF-8 particles must be large enough to seal the surface PEO pores on the surface and crystallisation of ZIF-8 throughout the entire thickness is also necessary. In this context, balancing PEO depletion with ZIF-8 formation is a key factor determining the performance of the final coating. Thus, among all coatings tested, the one obtained at 140 °C for 20 h provided the most effective protection. In turn, the protective ability of 140-5 was lower due to the lower amount of ZIF-8 present, i.e., fewer corrosion inhibitors can be released from the system. In the case of the 140-40 and 140-60 coatings, i.e., that have a high degree of PEO-to-ZIF-8 transformation, both demonstrated performance comparable to a 140-20 coating at the beginning of the immersion. However, this quickly dropped due to active ZIF-8 dissolution from the surface during corrosion. However, while the performance of the 140-40 material after 168 h of immersion was even worse than that of the untreated PEO specimen, for the 140-60 material it remained comparable. This result is most likely related to the sealing of the deep PEO pores in the 140-60 specimens, as shown by cross section analysis and 2D synchrotron mappings.

Discussing the photocatalytic and adsorption properties of the ZIF-8@PEO coatings, it should be noted, that the VST had a negative effect on both. These results differ from our previous investigations on the photocatalytic performance of ZIF-8@ZnO/$ZnAl_2O_4$-based PEO coatings [64] and powder ZIF-8@ZnO powder composites [66,88]. All these materials exhibited enhanced photocatalytic activity compared to systems that were not modified with ZIF-8. The negative effect as observed in the current study is most likely associated with the high level of the sealing of the PEO surface, and, consequently, with the blocking of MO access to ZnO, which is mainly responsible for the photocatalytic activity in the coatings. In that context, further investigationson optimisation are needed, as well as on understanding of the effect of ZIF-8.

4. Conclusions

The current investigation focused on the applying VST (vapour-solid transformation) method to PEO coatings based on ZnO on the surface of the Z1 Zn alloy. Under the applied conditions, the PEO layer was partially transformed into ZIF-8. Increasing both the reaction temperature from 120 °C to 150 °C and the reaction time from 5 h to 60 h resulted in a higher degree of the PEO-to-ZIF-8 transformation as well as in an increase of the amount and/or size of the surface ZIF-8 particles. Moreover, applying the VST method at elevated temperatures and for longer times led to the sealing of the PEO pores. While treatments at lower temperatures and times only sealed the surface pores, high temperatures and long VST led to the sealing of the both external and internal PEO pores. EIS tests demonstrated that the partial PEO-to-ZIF-8 transformation positively affected the protective ability of the coatings. The key factor determining the protective ability of the final coating was a balance between the decrease of amount of ZnO phase forming the PEO layer and the formation of ZIF-8.

Data availability

Data will be made available on request.

Declaration of competing interest

The authors declare that they have no known competing financial interests or personal relationships that could have appeared to influence the work reported in this paper.

Acknowledgements

Dr. Valeryia Kasneryk thanks Alexander von Humboldt Foundation for financial support. The authors acknowledge Deutsches Elektronen-Synchrotron (DESY, Hamburg, Germany) for the provision of experimental facilities. Part of this research was carried out at PETRA III, P.03 end-station: the beamtime was allocated for the proposals I-20211343 and I-20231247. The authors also thank Dr. Ting Wu, Mrs. Kristina Mojsilović, Mr. Volker Heitmann and Mr. Ulrich Burmester for the support in performing of the experiments.

Appendix A. Supplementary data

Supplementary data to this article can be found online at https://doi.org/10.1016/j.jmrt.2025.07.038.

References

[1] Mozumder MS, Mourad A-HI, Pervez H, Surkatti R. Recent developments in multifunctional coatings for solar panel applications: a review. Sol Energy Mater Sol Cell 2019;189:75–102.
[2] George JS, Vijayan PP, Hoang AT, Kalarikkal N, Nguyen-Tri P, Thomas S. Recent advances in bio-inspired multifunctional coatings for corrosion protection. Prog Org Coating 2022;168:106858.
[3] Ragesh P, Anand Ganesh V, Nair SV, Nair AS. A review on 'self-cleaning and multifunctional materials'. J Mater Chem A 2014;2:14773–97.
[4] Vishwakarma V, Kaliaraj GS, Amirtharaj Mosas KK. Multifunctional coatings on implant materials - a systematic review of the current scenario. Coatings 2023;13:69.
[5] Kozhukharov SV, Samichkov VI, Girginov CA, Machkova MS. Actual trends in the elaboration of advanced multifunctional coating systems for the efficient protection of lightweight aircraft alloys. Corrosion Rev 2017;35:383–96.
[6] Arunnellaiappan T, Rama Krishna L, Anoop S, Uma Rani R, Rameshbabu N. Fabrication of multifunctional black PEO coatings on AA7075 for spacecraft applications. Surf Coating Technol 2016;307:735–46.
[7] López-Ortega A, Sáenz de Viteri V, Alves SA, Mendoza G, Fuentes E, Mitran V, et al. Multifunctional TiO_2 coatings developed by plasma electrolytic oxidation technique on a Ti20Nb20Zr4Ta alloy for dental applications. Biomater Adv 2022;138:212875.

[8] Rokosz K, Hryniewicz T, Dudek Ł. Phosphate porous coatings enriched with selected elements via PEO treatment on titanium and its alloys: a review. Materials 2020;13:2468.
[9] Sikdar S, Menezes PV, Maccione R, Jacob T, Menezes PL. Plasma electrolytic oxidation (PEO) process—processing, properties, and applications. Nanomaterials 2021;11:1375.
[10] Wu T, Blawert C, Serdechnova M, Zheludkevich ML. Dissimilar metal joints on macro- and micro scales: impact on PEO processing-A review. J Mater Sci Technol 2025;211:30–52.
[11] Yerokhin AL, Nie X, Leyland A, Matthews A, Dowey SJ. Plasma electrolysis for surface engineering. Surf Coating Technol 1999;122:73–93.
[12] Matykina E, Arrabal R, Mohedano M, Mingo B, Gonzalez J, Pardo A, et al. Recent advances in energy efficient PEO processing of aluminium alloys. Trans Nonferrous Metals Soc China 2017;27:1439–54.
[13] Kasalica B, Petković-Benazzouz M, Sarvan M, Belča I, Maksimović B, Misailović B, et al. Mechanisms of plasma electrolytic oxidation of aluminum at the multi-hour timescales. Surf Coating Technol 2020;390:125681.
[14] Wang S, Liu X, Yin X, Du N. Influence of electrolyte components on the microstructure and growth mechanism of plasma electrolytic oxidation coatings on 1060 aluminum alloy. Surf Coating Technol 2020;381:125214.
[15] Jovović J, Stojadinović S, Šišović NM, Konjević N. Spectroscopic characterization of plasma during electrolytic oxidation (PEO) of aluminium. Surf Coating Technol 2011;206:24–8.
[16] Yang C, Chen P, Wu W, Sheng L, Zheng Y, Chu PK. A review of corrosion-resistant PEO coating on Mg alloy. Coatings 2024;14:451.
[17] Barati Darband G, Aliofkhazraei M, Hamghalam P, Valizade N. Plasma electrolytic oxidation of magnesium and its alloys: mechanism, properties and applications. J Magnesium Alloys 2017;5:74–132.
[18] Nadaraia KV, Suchkov SN, Imshinetskiy IM, Mashtalyar DV, Sinebrykhov SL, Gnedenkov SV. Some new aspects of the study of dependence of properties of PEO coatings on the parameters of current in potentiodynamic mode. Surf Coating Technol 2021;426:127744.
[19] Arrabal R, Matykina E, Hashimoto T, Skeldon P, Thompson GE. Characterization of AC PEO coatings on magnesium alloys. Surf Coating Technol 2009;203:2207–20.
[20] Gnedenkov AS, Sinebryukhov SL, Filonina VS, Plekhova NG, Gnedenkov SV. Smart composite antibacterial coatings with active corrosion protection of magnesium alloys. J Magnesium Alloys 2022;10:3589–611.
[21] Gnedenkov AS, Sinebryukhov SL, Filonina VS, Ustinov AY, Gnedenkov SV. Hybrid coatings for active protection against corrosion of Mg and its alloys. Polymers 2023;15:3035.
[22] Gnedenkov AS, Sinebryukhov SL, Filonina VS, Ustinov AY, Sukhoverkhov SV, Gnedenkov SV. New polycaprolactone-containing self-healing coating design for enhance corrosion resistance of the magnesium and its alloys. Polymers 2023;15:202.
[23] Aliofkhazraei M, Macdonald DD, Matykina E, Parfenov EV, Egorkin VS, Curran JA, et al. Review of plasma electrolytic oxidation of titanium substrates: mechanism, properties, applications and limitations. Appl Surf Sci Adv 2021;5:100121.
[24] Santos-Coquillat A, Martínez-Campos E, Mohedano M, Martínez-Corriá R, Ramos V, Arrabal R, et al. In vitro and in vivo evaluation of PEO-modified titanium for bone implant applications. Surf Coating Technol 2018;347:358–68.
[25] Fattah-alhosseini A, Molaei M, Babaei K. The effects of nano- and micro-particles on properties of plasma electrolytic oxidation (PEO) coatings applied on titanium substrates: a review. Surf Interfaces 2020;21:100659.
[26] Blawert C, Karpushenkov SA, Serdechnova M, Karpushenkava LS, Zheludkevich ML. Plasma electrolytic oxidation of zinc alloy in a phosphate-aluminate electrolyte. Appl Surf Sci 2020;505:144552.
[27] Stojadinović S, Tadić N, Vasilić R. Formation and characterization of ZnO films on zinc substrate by plasma electrolytic oxidation. Surf Coating Technol 2016;307:650–7.
[28] Joseph J, Gallo SC, Catubig R, Wang K, Somers A, Howlett P, et al. Formation of a corrosion-resistant coating on zinc by a duplex plasma electrolytic oxidation and conversion surface treatment. Surf Coating Technol 2020;395:125918.
[29] Stojadinović S, Radić N, Vasilić R. ZnO particles modified MgAl coatings with improved photocatalytic activity formed by plasma electrolytic oxidation of AZ31 magnesium alloy in aluminate electrolyte. Catalysts 2022;12:1503.
[30] Han Q, Li Y, Lu X, Mei D, Chen Q, Zhang T, et al. Fabrication of Ag containing antibacterial PEO coatings on pure Mg. Mater Lett 2021;293:129731.
[31] Cerchier P, Pezzato L, Brunelli K, Dolcet P, Bartolozzi A, Bertani R, et al. Antibacterial effect of PEO coating with silver on AA7075. Mater Sci Eng C 2017;75:554–64.
[32] Ghanbari A, Bordbar-Khiabani A, Warchomicka F, Sommitsch C, Yarmand B, Zamanian A. PEO/Polymer hybrid coatings on magnesium alloy to improve biodegradation and biocompatibility properties. Surf Interfaces 2023;36:102495.
[33] Yu K, Li P, Han Q, Wang Q, Karpushenkov SA, Lu X, et al. Investigation of biodegradability, cytocompatibility and antibacterial property of plasma electrolytic oxidation coating on Mg. Surf Interfaces 2022;30:101840.
[34] Mashtalyar DV, Nadaraia KV, Plekhova NG, Imshinetskiy IM, Piatkova MA, Pleshkova AI, et al. Antibacterial Ca/P-coatings formed on Mg alloy using plasma electrolytic oxidation and antibiotic impregnation. Mater Lett 2022;317:132099.
[35] Zhang X, Aliasghari S, Němcová A, Burnett TL, Kuběna I, Šmíd M, et al. X-Ray computed tomographic investigation of the porosity and morphology of plasma electrolytic oxidation coatings. ACS Appl Mater Interfaces 2016;8:8801–10.
[36] Vaghefinazari B, Lamaka SV, Gazenbiller E, Yasakau K, Blawert C, Serdechnova M, et al. Corrosion inhibition of decylphosphonate on bare and PEO-coated Mg alloy. Corros Sci 2024;226:111651.
[37] Yang J, Blawert C, Lamaka SV, Snihirova D, Lu X, Di S, et al. Corrosion protection properties of inhibitor containing hybrid PEO-epoxy coating on magnesium. Corros Sci 2018;140:99–110.
[38] Gnedenkov AS, Filonina VS, Sinebryukhov SL, Gnedenkov SV. A superior corrosion protection of Mg alloy via smart nontoxic hybrid inhibitor-containing coatings. Molecules 2023;28:2538.
[39] Gnedenkov AS, Kononenko YI, Sinebryukhov SL, Filonina VS, Vyaliy IE, Nomerovskii AD, et al. The effect of smart PEO-coatings impregnated with corrosion inhibitors on the protective properties of AlMg3 aluminum alloy. Materials 2023;16:2215.
[40] Bordbar-Khiabani A, Yarmand B, Sharifi-Asl S, Mozafari M. Improved corrosion performance of biodegradable magnesium in simulated inflammatory condition via drug-loaded plasma electrolytic oxidation coatings. Mater Chem Phys 2020;239:122003.
[41] Montemor MF. Functional and smart coatings for corrosion protection: a review of recent advances. Surf Coating Technol 2014;258:17–37.
[42] Grigoriev D, Shchukina E, Shchukin DG. Nanocontainers for self-healing coatings. Adv Mater Interfac 2017;4:1600318.
[43] Chen Q, Lu X, Serdechnova M, Wu T, Wieland DCF, Kasneryk V, et al. Synergistic chelating agents for in-situ synthesis of Mg-Al LDH films on PEO treated Mg alloy. J Magnesium Alloys 2024.
[44] Chen Q, Lu X, Serdechnova M, Wu T, Kasneryk V, Naacke T, et al. Insights into in-situ synthesis of PEO-LDH composite film on AM50 Mg alloy: the effect of final voltage. Surf Coating Technol 2024;485:130907.
[45] Shulha T, Shikun M, Serdechnova M, Naacke T, Kasneryk V, Heitmann V, et al. Chelating agent stimulated LDH post-treatment of PEO coated AA2024. Appl Surf Sci 2024;670:160707.
[46] del Olmo R, Mohedano M, Mingo B, Arrabal R, Matykina E. LDH post-treatment of flash PEO coatings. Coatings 2019;9:354.
[47] Zhang D, Zhou J, Peng F, Tan J, Zhang X, Qian S, et al. Mg-Fe LDH sealed PEO coating on magnesium for biodegradation control, antibacteria and osteogenesis. J Mater Sci Technol 2022;105:57–67.
[48] Zhang Y, Yu P, Zuo Y, Tian H, Chen X, Chen F. Investigating the growth behavior of LDH layers on MAO-coated aluminum alloy: influence of microstructure and surface element. Int J Electrochem Sci 2018;13:610–20.
[49] Nikoomanzari E, Fattah-alhosseini A. Maximizing the potential applications of plasma electrolytic oxidation coatings produced on Mg-based alloys in anti-corrosion, antibacterial, and photocatalytic targeting through harnessing the LDH/PEO dual structure. J Magnesium Alloys 2024;12:2674–94.
[50] Kasneryk V, Serdechnova M, Blawert C, Zheludkevich ML. LDH has been grown: what is next? Overview on methods of post-treatment of LDH conversion coatings. Appl Clay Sci 2023;232:106774.
[51] Serdechnova M, Mohedano M, Kuznetsov B, Mendis CL, Starykevich M, Karpushenkov S, et al. PEO coatings with active protection based on in-situ formed LDH-nanocontainers. J Electrochem Soc 2017;164:C36–45.
[52] Chen F, Yu P, Zhang Y. Healing effects of LDHs nanoplatelets on MAO ceramic layer of aluminum alloy. J Alloys Compd 2017;711:342–8.
[53] Liu G, Lu X, Zhang X, Zhang T, Wang F. Improvement of corrosion resistance of PEO coatings on Al alloy by formation of ZnAl layered double hydroxide. Surf Coating Technol 2022;441:128528.
[54] Zhang G, Jiang E, Wu L, Tang A, Atrens A, Pan F. Active corrosion protection of phosphate loaded PEO/LDHs composite coatings: SIET study. J Magnesium Alloys 2022;10:1351–7.
[55] Zhang G, Wu L, Tang A, Ma Y, Song G-L, Zheng D, et al. Active corrosion protection by a smart coating based on a MgAl-layered double hydroxide on a cerium-modified plasma electrolytic oxidation coating on Mg alloy AZ31. Corros Sci 2018;139:370–82.
[56] Zhao C, Wang X, Li C, Liu Y, Sun S, Yang S, et al. Superior tribological and anti-corrosion performance of corrosion inhibitors intercalated LDH-MAO coating on AZ31 Mg alloys. Tribol Int 2024;191:109126.
[57] Gnedenkov AS, Sinebryukhov SL, Nomerovskii AD, Filonina VS, Ustinov AY, Gnedenkov SV. Design of self-healing PEO-based protective layers containing in-situ grown LDH loaded with inhibitor on the MA8 magnesium alloy. J Magnesium Alloys 2023.
[58] Zhang Z-Y, Lu S, Lv W-G, Gu J-J, Zhou S-F, Zhang J-W, et al. Enhanced corrosion resistance and biofunctionality of Zn–Al layered double hydroxide coating on micro-arc oxidized ZK60 Mg alloy via ion exchange. Mater Chem Phys 2023;299:127482.
[59] Stock N, Biswas S. Synthesis of metal-organic frameworks (MOFs): routes to various MOF topologies, morphologies, and composites. Chem Rev 2012;112:933–69.
[60] Rani P, Kasneryk V, Opanasenko M. MOF-inorganic nanocomposites: bridging a gap with inorganic materials. Appl Mater Today 2022;26:101283.
[61] Lee Y-R, Kim J, Ahn W-S. Synthesis of metal-organic frameworks: a mini review. Kor J Chem Eng 2013;30:1667–80.
[62] Xu K, Zhang S, Zhuang X, Zhang G, Tang Y, Pang H. Recent progress of MOF-functionalized nanocomposites: from structure to properties. Adv Colloid Interface Sci 2024;323:103050.
[63] Zhu Q-L, Xu Q. Metal–organic framework composites. Chem Soc Rev 2014;43:5468–512.
[64] Kasneryk V, Wu T, Rohr H, Serdechnova M, Mojsilović K, Florian Wieland DC, et al. Controllable recrystallization of ZnO/$ZnAl_2O_4$ based PEO into ZIF-8 as a route for the formation of multifunctional coatings. J Ind Eng Chem 2024;132:395–409.
[65] Telmenbayar L, Gopal Ramu A, Yang D, Choi D. Development of mechanically robust and anticorrosion slippery PEO coating with metal–organic framework (MOF) of magnesium alloy. Chem Eng J 2023;458:141397.

[66] Jiang S, Zhang Z, Wang D, Wen Y, Peng N, Shang W. ZIF-8-based micro-arc oxidation composite coatings enhanced the corrosion resistance and superhydrophobicity of a Mg alloy. J Magnesium Alloys 2023;11:1367–80.
[67] Zhang H, Zhao M, Lin YS. Stability of ZIF-8 in water under ambient conditions. Microporous Mesoporous Mater 2019;279:201–10.
[68] Chen B, Yang Z, Zhu Y, Xia Y. Zeolitic imidazolate framework materials: recent progress in synthesis and applications. J Mater Chem A 2014;2:16811–31.
[69] Li Y, Ma C, Nian P, Liu H, Zhang X. Green synthesis of ZIF-8 tubular membranes from a recyclable 2-methylimidazole water-solvent solution by ZnO nanorods self-converted strategy for gas separation. J Membr Sci 2019;581:344–54.
[70] Wang Q, Sun Y, Li S, Zhang P, Yao Q. Synthesis and modification of ZIF-8 and its application in drug delivery and tumor therapy. RSC Adv 2020;10:37600–20.
[71] Zhang J, Tan Y, Song W-J. Zeolitic imidazolate frameworks for use in electrochemical and optical chemical sensing and biosensing: a review. Microchim Acta 2020;187:234.
[72] Park KS, Ni Z, Côté AP, Choi JY, Huang R, Uribe-Romo FJ, et al. Exceptional chemical and thermal stability of zeolitic imidazolate frameworks. Proc Natl Acad Sci 2006;103:10186–91.
[73] Jiang L, Dong Y, Yuan Y, Zhou X, Liu Y, Meng X. Recent advances of metal–organic frameworks in corrosion protection: from synthesis to applications. Chem Eng J 2022;430:132823.
[74] Kasneryk V, Poschmann MPM, Serdechnova M, Dovzhenko G, Wieland DCF, Karlova P, et al. Formation and structure of ZIF-8@PEO coating on the surface of zinc. Surf Coating Technol 2022;445:128733.
[75] Pola A, Tocci M, Goodwin FE. Review of microstructures and properties of zinc alloys. Metals 2020;10:253.
[76] Poschmann MPM, Siebert L, Lupan C, Lupan O, Schütt F, Adelung R, et al. Surface conversion of ZnO tetrapods produces pinhole-free ZIF-8 layers for selective and sensitive H2 sensing even in pure methane. ACS Appl Mater Interfaces 2023;15:38674–81.
[77] Collins TJ. ImageJ for microscopy. Biotechniques 2007;43:S25–30.
[78] Krywka C, Neubauer H, Priebe M, Salditt T, Keckes J, Buffet A, et al. A two-dimensional waveguide beam for X-ray nanodiffraction. J Appl Crystallogr 2012;45:85–92.
[79] Wu T, Blawert C, Serdechnova M, Karlova P, Dovzhenko G, Wieland DCF, et al. PEO processing of AZ91Nd/Al2O3 MMC-the role of alumina fibers. J Magnesium Alloys 2021;10:423–39.
[80] Ashiotis G, Deschildre A, Nawaz Z, Wright JP, Karkoulis D, Picca FE, et al. The fast azimuthal integration Python library: pyFAI. J Appl Crystallogr 2015;48:510–9.
[81] Serdechnova M, Blawert C, Karpushenkov S, Karpushenkava L, Shulha T, Karlova P, et al. Properties of ZnO/$ZnAl_2O_4$ composite PEO coatings on zinc alloy Z1. Surf Coating Technol 2021;410:126948.
[82] Banaś J, Stypuła B, Banaś K, Światowska-Mrowiecka J, Starowicz M, Lelek-Borkowska U. Corrosion and passivity of metals in methanol solutions of electrolytes. J Solid State Electrochem 2009;13:1669–79.
[83] Banaś J, Schütze KG, Heitz E. Corrosion studies on zinc in a methanol/water/lithium chloride/oxygen system. J Electrochem Soc 1986;133:253.
[84] Wang L, Kang B, Gao N, Du X, Jia L, Sun J. Corrosion behaviour of austenitic stainless steel as a function of methanol concentration for direct methanol fuel cell bipolar plate. J Power Sources 2014;253:332–41.
[85] Chen Y, Wu L, Wu M, Yao W, Wu J, Zhou Y, et al. Preparation and corrosion behavior of MAO based MOFs coatings with excellent film-forming and adhesion properties. Surf Coating Technol 2024;493:131246.
[86] Perrot V, Roussey A, Benayad A, Veillerot M, Mariolle D, Solé-Daura A, et al. ZIF-8 thin films by a vapor-phase process: limits to growth. Nanoscale 2023;15:7115–25.
[87] Chakraborty B, Schadte P, Poschmann MPM, Lupan C, Zadorojneac T, Magariu N, et al. MOF-coated 3D-printed ZnO tetrapods as a two-in-one sensor for H_2 sensing and UV detection. In: Sontea V, Tiginyanu I, Railean S, editors. 6th international conference on nanotechnologies and biomedical engineering. Cham: Springer Nature Switzerland; 2024. p. 70–9.
[88] Zheng H-b, Wu D, Wang Y-l, Liu X-p, Gao P-z, Liu W, et al. One-step synthesis of ZIF-8/ZnO composites based on coordination defect strategy and its derivatives for photocatalysis. J Alloys Compd 2020;838:155219.